Journal of Magnetic Resonance 199 (2009) 188–191

Contents lists available at ScienceDirect

Journal of Magnetic Resonance

journal homepage: www.elsevier.com/locate/jmr

MRI with an atomic magnetometer suitable for practical imaging applications

I.M. Savukov *, V.S. Zotev, P.L. Volegov, M.A. Espy, A.N. Matlashov, J.J. Gomez, R.H. Kraus Jr.

Los Alamos National Laboratory, Los Alamos, NM 87544, USA

ARTICLE INFO

Article history:
Received 4 February 2009
Revised 22 April 2009
Available online 3 May 2009

Keywords:
MRI
Ultra-low field
Atomic magnetometer
SQUID

ABSTRACT

Conventionally implemented MRI is performed in a strong magnetic field, typically >1 T. The high fields, however, can lead to many limitations. To overcome these limitations, ultra-low field (ULF) [or microtesla] MRI systems have been proposed and implemented. To-date such systems rely on low-Tc Superconducting Quantum Interference Devices (SQUIDs) leading to the requirement of cryogens. In this letter, we report ULF–MRI obtained with a non-cryogenic atomic magnetometer. This demonstration creates opportunities for developing inexpensive and widely applicable MRI scanners.

Published by Elsevier Inc.

MRI is widely used and considered a routine and powerful diagnostic procedure. Nonetheless, traditional MRI has limitations and difficulties. For example, wider availability of MRI is impeded by the high cost of the instrumentation and the need for large and heavy superconducting or permanent magnets. To solve these problems, inexpensive systems based on ultra-low field (ULF)–MRI methods have been proposed where scans can be performed without such magnets [1]. Experimentally, ULF–MRI systems were implemented and successfully applied to imaging with low-Tc SQUIDs [2–6], including imaging of human brain [7]. In addition to the advantages in simplicity of magnetic field generation, safety, and cost, the open design of ULF–MRI systems allows more flexible positioning of patients, a particularly important advantage if such positioning is required by patient condition, treatment or surgical procedure. Moreover, ULF–MRI is less restrictive for combining with various other imaging modalities. It also has potential diagnostic and scientific advantages that can provide totally new information. For example, ULF–MRI can be effectively combined with magnetoencephalography (MEG) to reduce co-registration errors [7]. There is indication that abnormal tissues such as tumors exhibit greater T_1 (longitudinal relaxation time) contrast at low field, and such anomalies can be revealed without injection of gadolinium-based contrast agents [6], which can have long term adverse effects [8]. In general T_1 of water and tissues [9,10] depends on magnetic field and NMR frequency, and differences in T_1 (contrast) increase at low fields. ULF–NMR is also sensitive to processes at ms time scale, including protein folding, and can be used for studying such processes [11]. Our group is working on exploiting the idea of direct neural imaging (DNI) with ULF–MRI based on a resonant absorption mechanism that provides enhancement in sensitivity [12].

Thus far, these multiple applications of ULF–MRI relied on low-Tc SQUIDs. However, with the advent of ultra-sensitive atomic magnetometers (AMs) of comparable sensitivity [13] it has become possible to develop similar applications without SQUIDs and cryogens. The first NMR detection with an AM was reported in 2005 [14]. However, this and the following NMR and MRI experiments [15,16] were based on liquid flow and were not readily applicable to biomedical anatomical imaging. Liquid flow was needed to meet the requirement of prepolarization, which is necessary in low-field MRI because the signal otherwise would be extremely small. Water was arranged to flow in a tubing from an external permanent magnet through a narrow opening inside a mu-metal shield where the atomic cell of an AM was located, and such arrangement is impossible for general anatomical imaging, except to image some blood vessels. However if the magnet is moved inside the shield to locally spin-polarize a subject (as would be required in MRI of living subjects), the AM would not operate in the proximity of this magnet due to its sensitivity to magnetic fields and gradients. Even with a pulsed prepolarizing coil, the operation of the AM will be problematic because of residual magnetization of the mu-metal shield. NMR detection with an AM more relevant to anatomical imaging was demonstrated only in 2007 [17], but this work did not address the problem of how to detect the AM signal in the presence of magnetic gradients required for MRI. The field separation technique (required because MRI and AM fields have to differ by three orders of magnitude) was furthermore not conducive to typical MRI of living subjects. In this work, we demonstrate MRI with an AM that can be developed into practical anatomical imaging. Although in the current demonstration the resolution and signal-to-noise ratio (SNR) of the MRI are not yet sufficient for clinical applications, it

* Corresponding author.
E-mail address: isavukov@lanl.gov (I.M. Savukov).

1090-7807/$ - see front matter Published by Elsevier Inc.
doi:10.1016/j.jmr.2009.04.012

constitutes the proof of principle that a non-cryogenic MRI system based on an AM can be built. A clear path is outlined for achieving this goal. The requirements for sensitivity and the feasibility of achieving necessary MRI resolution and SNR are analyzed.

In addition to the most well known and arguably most important medical imaging applications, MRI scanners are also used in other applications including industrial scanning of materials, security applications, and many others. The imaging quality required for most medical applications would need to demonstrate resolution on the order of 1 mm and SNR per voxel of about 30 for a reasonable imaging time on the order of 10 min [18]. In our previous demonstration of ULF–MRI, we used a 7-channel SQUID system with a typical 3 fT/Hz$^{1/2}$ sensitivity and a 0.03 T prepolarization field [7]. A 90 min scan was required to achieve a head image with $3 \times 3 \times 6$ mm spatial resolution and SNR ≈30. By scaling this result, we estimate that achieving clinically relevant ULF–MRI imaging quality for a reasonable scan time (10 min) would require a 0.1 T prepolarization field, 0.2 fT/Hz$^{1/2}$ sensitivity using multiple channel acquisition. Attaining the specified sensitivity is a key to realizing a practical ULF–MRI system. This is why the most sensitive detectors, such as SQUIDs or AMs, must be employed. Although it is clear that the higher detector sensitivity the better is SNR per voxel in MRI, it is less obvious why multi-channel configuration of detectors have to be used. The reason for this is that smaller-diameter coils generate larger signals without noise increase from small voxels located in the vicinity of the coils, and hence multiple small-diameter coils can produce better SNR per voxel than a single larger-diameter coil covering the same sample area. This can be understood from the principle of reciprocity that states that the flux through a coil from a source with a given magnetization is proportional to the field per unit current produced by the coil in the voxel location. Because the field of a coil scales inversely with the coil diameter, a smaller coil outputs a larger signal per voxel of MRI sample in its vicinity. In other words, filling factor for a small voxel is higher for a small than large coil. The drawback of a small coil is that its field of view is very limited, so a small coil cannot be used alone to image a large area. Instead an array of coils has to be used. The solution is an array of coils that can cover the entire MRI area.

We conducted MRI experiments with an AM to better understand the practical problems of applying AMs in MRI and to show a practical example of working system. In the experiments we used our SQUID ULF–MRI system installed inside a double-layer magnetically shielded room with the following MRI protocol (see Ref. [5] for details). The prepolarizing field B_p (35 mT) was applied in the vertical (y) direction for about 1.5 s to polarize the sample (a bottle of diameter 2 cm and length 3 cm filled with tap water) and turned off with a ramp down of 6 ms. After a small delay (10 ms), a measurement field B_m, which was perpendicular to B_p, was applied, causing the nuclear spins to precess around B_m as if excited by a $\pi/2$ pulse. Frequency-encoding $G_x = dB_z/dx$ and phase-encoding $G_z = dB_z/dz$ gradients were applied for 2D imaging. The G_x (5 Hz/cm) gradient was turned on simultaneously with B_m, and its polarity was reversed after 0.5 s to produce a gradient echo at 1 s. The G_z gradient was applied simultaneously with the positive lobe of G_x and its value was changed in 17 steps from −5 Hz/cm to 5 Hz/cm. The MRI pulses, signal acquisition, and data processing were fully automated.

For the detection of ULF–MRI signals by an AM, we constructed a portable AM which can be moved in and out of the shielded room. The AM principles and design are similar to those described previously [17,19], but some new features were added which are described below. The AM consists of a 1-cm cubic atomic cell containing a drop of K, 75.5 kPa of ^{4}He, 5.5 kPa of N_2; two lasers (770 nm, 40 mW power) to provide optical pumping of K spins and to measure their precession; optics, and electronics. The cell and a glass oven, designed to heat the cell (Fig. 1), are enclosed in a small ferrite box, which reduces external magnetic field 100 times to make the operation of the magnetometer more sensitive and stable whether used inside or outside the shielded room. The ferrite box was used in our MRI experiments to minimize the effects of MRI fields and gradients when the AM was inside the shielded room. Ferrite was chosen because of its low magnetic noise [20]. The AM Zeeman resonance was tuned by applying a bias field, about 4×10^{-7} T. For optimal performance, the atomic cell was electrically heated to a temperature 200 °C inside an oven. Since the current through the heating elements creates significant magnetic field, it was turned off during measurement time with a solid-state switch. Except for the first 50 ms after the heater was turned off, the AM sensitivity was the same as when the heater was completely disconnected. Batteries were used to power the heater inside the shielded room to minimize magnetic noise.

A significant impediment to MRI with an AM is that an AM is sensitive to MRI fields and gradients, and at least one field B_m and one gradient G_x are present during the data acquisition cycle. To solve this, we added a flux transformer (FT) to the AM setup (Fig. 1). The input coil of the FT (230 turns, 7.5 cm diameter, 0.83 mm copper wire diameter, resistance 1.8 Ω, inductance 3.8 mH) was located near a water phantom, in the center of the MRI coils. The output coil (40 turns, 5.5 cm diameter, 0.25 mm copper wire diameter, 3 Ω resistance with connecting ends) was mounted inside the AM ferrite shield on the external surface of the oven, slightly above the center so as not to block the probe and pump beams passing through the cell. These parameters of the FT were chosen without thorough sensitivity optimization, which is the future goal, but with some consideration of noise and geometry. In particular, the input coil was chosen to fit between the Dewar and prepolarization coil, to allow simultaneous AM and SQUID recording, and the output coil was chosen to fit inside the ferrite shield. We chose the coils' numbers of turns with a capacitor added in sequence to have magnetic field amplification coefficient high enough that AM noise would not exceed the thermal noise of the FT in the output coil. Theory of noise of the AM + FT system is provided below. The AM was about 1 m away from the MRI coils. The FT functions in the following way. The time-varying magnetic flux (DC field does not produce any signal) from precessing nuclear spins of water produces AC voltage in the input coil and drives a current through the output coil. The current generates a magnetic field in the output coil which is detected by the AM. In the future, we plan to arrange many FTs with a multichannel AM to enhance SNR and accelerate MRI. Although we expect some problem due to interaction between coils, we can solve this problem by using similar parallel MRI approaches as in Ref. [5]. The coupling between pick-up coils in Ref. [5] was on the order of

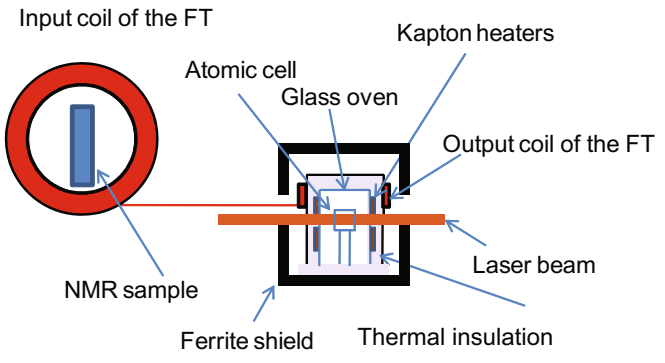

Fig. 1. The detection system based on the flux transformer and the atomic magnetometer.

1–2 per cent, and we can arrange our coil to have similar coupling coefficients. There is also possibility to use current feedback in coils to minimize interaction between coils.

With the aid of the FT, the AM was used simultaneously with our 7-channel SQUID system to obtain comparative ULF–MR images from both sensor systems. The AM was inserted half way through the window in the shielded room to have its sensitive part, the atomic cell, inside the room, while keeping the magnetic noise generating parts, the lasers and their electronics, outside. We also oriented the input coil of the FT perpendicular to the B_p and B_m coils to minimize pickup of switching related transients by the FT and the SQUIDs. With this arrangement we obtained artifact-free MR images. Initially, we acquired MRIs at 1.945 kHz, a frequency that was far from optimal for the AM, but at which our SQUID-based ULF–MRI system normally operated. To investigate if quality of MRI improves with frequency, which is expected according to Eq. (2), we conducted another MRI experiment at higher frequency, 3.2 kHz. We found that the quality of the image obtained with the AM greatly improved and became comparable to that of the image obtained with the central SQUID (Fig. 2), which has about 1 fT/Hz$^{1/2}$ sensitivity. Such rapid improvement with frequency suggests that at high frequencies it should be possible to exceed the quality of images obtained with our state-of-the-art commercial SQUIDs. While 2D, 2 mm image resolution demonstrated here can already be useful for some imaging applications, the value for general anatomical imaging is suboptimal. Further significant progress is expected based on the analysis of sensitivity provided below.

The input sensitivity of the AM + FT system depends on the noise of the FT (δB_{FT}), its field enhancement coefficient ($k_{FT} = B_{out}/B_{in}$), and the sensitivity of the AM (δB_{AM}):

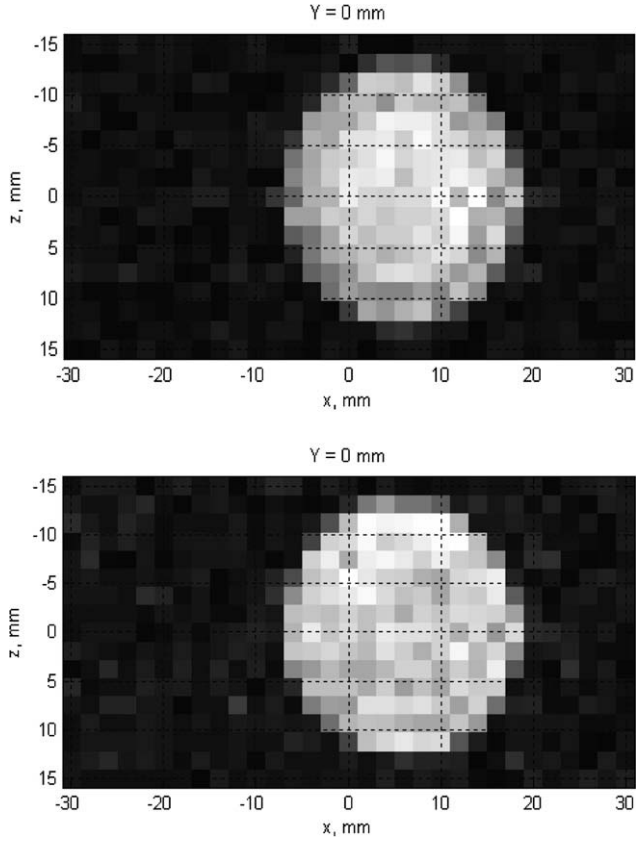

Fig. 2. MR images of a water phantom obtained with a SQUID (the top panel) and an AM (the bottom panel) at 3.2 kHz. Imaging time is 12 min.

$$\delta B = \sqrt{\delta B_{FT}^2 + (\delta B_{AM}/k_{FT})^2}. \quad (1)$$

The noise of the FT is the combined Johnson noise of its two coils,

$$\delta B_{FT} = \frac{8}{\omega D_{in}}\sqrt{\frac{k_B T_{in}\rho_{in}}{\pi D_{in} A_{in}}}\sqrt{1 + T_{out}R_{out}/T_{in}R_{in}}, \quad (2)$$

where A_{in}, D_{in}, T_{in}, ρ_{in}, and R_{in} are the winding cross-section area, average diameter, absolute temperature, resistivity, and resistance of the input coil; T_{out} and R_{out} are the temperature and the resistance of the output coils; ω is the angular frequency. All quantities are expressed in SI units. The result does not include skin-depth and proximity effects, but they can be minimized by using narrow-gauge Litz wire [17], at least at frequencies below a few MHz. The Johnson noise of the FT used to obtain the water phantom MRI was 12 fT/Hz$^{1/2}$ at 3.2 kHz. The Johnson noise can be substantially improved over this first proof-of-principle FT. We estimate that a sensitivity of 0.2 fT/Hz$^{1/2}$ is possible for a coil with the cross-section of 10 cm^2 at 30 kHz. This is our future goal for creating a competitive MRI scanner. Even further improvement in sensitivity can be achieved by increasing the frequency and the cross-section, but there are some limiting factors. In particular, high MRI frequency requires higher uniformity and stability of the B_m field, which are not readily achieved. Furthermore, background noise is not necessarily better at higher frequencies as observed in our lab: magnetic field noise was 10 fT/Hz$^{1/2}$ at 30 kHz, but significantly increased at 40–60 kHz. We found that 30 kHz frequency is practical for an MRI scanner. For example, a Helmholtz coil system, among the best simple systems, of the size 1 m can generate measurement field of uniformity better than 1 part in 1000 for a 20-cm sample and can be used for head imaging at 30 kHz, but higher frequency would require more elaborate field generation.

The number of turn in coils is another important factor that can affect the coil thermal noise through the effect of distributed capacitance and self-resonance. Unfortunately, this effect is not known quantitatively. We conducted several experiments to investigate this effect. We found that for a given frequency, the intrinsic coil noise was much greater than that predicted by Eq. (2). We further found that at a fixed coil cross-section the noise began to approach the theoretical value as the number of turns was reduced. As the result of our investigation, we concluded that a coil of 10 cm^2 at frequencies near 30 kHz must have fewer than 50 turns to prevent adversely affecting its noise performance. Thus there will be limits on the use of an amplifier, which otherwise might be a possible alternative. To illustrate this point, consider a practical coil with intrinsic sensitivity of 0.2 fT/Hz$^{1/2}$ (D_{in} = 10 cm, A_{in} = 10 cm^2, copper wire, 50 turns, R = 0.01 Ω). This coil is expected to have Johnson noise $\sqrt{4k_BTR} = 10$ pV/Hz$^{1/2}$, which is below that of the most sensitive commercial amplifiers, such as an amplifier sold by DL Instruments (Model 565) [22]. With a carefully designed and shielded ferrite transformer it has a noise level 0.15 nV/Hz$^{1/2}$. This amplifier could, in principle, be used by resonating the coil with a capacitor. However, resonant operation of the pickup would severely limit the use of this sensor by preventing the use of multiple coils for parallel MRI acceleration and employing background subtraction techniques using gradiometers or reference channels. Such limitations are, in our opinion, not desirable for most MRI scanner applications.

For the optimization of the cross-section, it is necessary to remember that a coil has a transient time that grows with the cross-section, $\tau = L/R \approx 3 \times 10^{-7} A/\rho$. (This equation was obtained using $R = \pi D\rho N^2/A$ and $L \approx 1.0 \times 10^{-6} DN^2$, where the inductance expression is the approximation of the expression given in Ref. [21] in the assumption that the diameter of the coil D is much larger than the efficient diameter of the cross-section area and that the slow logarithmic dependence in the expression of Ref. [21]

can be replaced by the constant equal to the value of the logarithm for our typical coil of interest with $D = 8$ cm and $A = 4$ cm^2.) The large pulses of magnetic field present in MRI can lead to long transients, which can raise the noise level during acquisition time. However, substantial suppression of transients can be achieved with the addition of a resistor (with a switch to disconnect resistor at measurement time) in parallel to damp transients. The resistor value must be greater than the coil's own resistance but smaller than the impedance of the coil, including a parasitic capacitance. Because decay time L/R with the resistor can be made much shorter, the energy would dissipate exponentially to a negligible level even in a large coil.

The field enhancement k_{FT} of a FT can be found from the ratio of the output $F_{out} = N_{out}A_{out}B_{\mathrm{out}}$ and input $F_{in} = N_{in}A_{in}B_{\mathrm{in}}$ fluxes:

$$\frac{F_{out}}{F_{in}} = \frac{j\omega L_{out}}{j\omega(L_{in} + L_{out}) + R - j/\omega C}, \tag{3}$$

where L_{in}, N_{in}, A_{in} and L_{out}, N_{out}, A_{out} are the inductances, the number of turns, and areas of the input and output coils, R is the FT total resistance, and C is a capacitance optionally added in sequence with the coils. At resonance $\omega(L_{in} + L_{out}) = 1/\omega C$ the output flux can be enhanced Q times compared to the no-capacitance case, where Q is the quality factor. Resonance would lower demand on the AM sensitivity, but significant current will flow in the coil and if multiple coils are used, strong coupling will occur. Hence resonance operation can be used only for a system with a single or weakly coupled coils. In our experiment, we used a FT with $Q = 15$ and the field enhancement was 6. The sensitivity of the system was not limited by the input coil of the FT.

The sensitivity of an AM at high frequencies was analyzed in Ref. [19]. From the analysis it follows that an optimized AM with an atomic cell volume 1 cm^3 can have a 0.1 fT/Hz$^{1/2}$ sensitivity, provided instrumental and magnetic-field noises are suppressed, which should be possible at 30 kHz frequency. With FT field enhancement greater than 1 (readily achievable, even without resonant operation), the sensitivity of FT + AM system can be made 0.2 fT/Hz$^{1/2}$ using the coil of 10 cm^2 cross-section analyzed here. Even higher sensitivity can be achieved, if larger FT coils are used.

In summary, we have demonstrated the first MRI with an AM that is directly relevant to the demands of practical anatomical imaging. The quality of images obtained even with our very simple, poorly optimized system is approaching that of SQUIDs and significant improvement is possible by increasing the prepolarization field, NMR frequency, coil cross-section and applying parallel MRI methods. An MRI–AM scanner based on the principle described here will have many advantages over conventional high-field scanners such as safety, portability, low cost, compatibility with other systems, flexibility in applications. We believe our approach is immediately suitable for deployment in many medical, industrial, and security applications such as detecting liquid explosives in airports or in food inspection.

Acknowledgment

This work was supported by the LANL LDRD program.

References

[1] A. Macovski, S. Conolly, Novel approaches to low-cost MRI, Magn. Reson. Med. 30 (1993) 221–230.
[2] R. McDermott et al., Liquid-state NMR and scalar couplings in microtesla magnetic fields, Science 295 (2002) 2247.
[3] R. McDermott et al., Mircotesla MRI with a superconducting quantum interference device, Proc. Natl. Acad. Sci. USA 201 (2004) 7851.
[4] Volegov et al., Simultaneous magnetoencephalography and SQUID detected nuclear MR in microtesla magnetic fields, Magn. Reson. Med. 52 (2004) 467–470.
[5] V.S. Zotev et al., Parallel MRI at microtesla fields, JMR 192 (2008) 197.
[6] J. Clarke, M. Hatridge, M. Moessle, SQUID-detected magnetic resonance imaging in microtesla fields, Annu. Rev. Biomed. Eng. 9 (2007) 389.
[7] V.S. Zotev et al., Microtesla MRI of the human brain combined with MEG, JMR 194 (2008) 115–120.
[8] D.R. Martin, Nephrogenic system fibrosis: a radiologist's practical perspective, Eur. J. Radiol. 66 (2008) 220–224.
[9] R.G. Bryant, D.A. Mendelson, C.C. Lester, The magnetic field dependence of proton spin relaxation in tissues, Magn. Reson. Med. 21 (1991) 117–126.
[10] B. Halle, Molecular theory of field-dependent proton spin–lattice relaxation in tissue, Magn. Reson. Med. 56 (2006) 60–72.
[11] J. Cavanagh, R.A. Venters, Protein dynamic studies move to a new time slot, Nat. Struct. Biol. 8 (2001) 912–914.
[12] R.H. Kraus Jr., P. Volegov, A. Matlachov, M. Espy, Toward direct neural current imaging by resonant mechanisms at ultra-low field, NeuroImage 39 (2009) 310–317.
[13] I.K. Kominis, T.W. Kornack, J.C. Allred, M.V. Romalis, A subfemtotesla multichannel atomic magnetometer, Nature 422 (2003) 596–599.
[14] I.M. Savukov, M.V. Romalis, NMR detection with an atomic magnetometer, Phys. Rev. Lett. 94 (2005) 123001.
[15] S. Xu et al., Construction and applications of an atomic magnetic gradiometer based on nonlinear magneto-optical rotation, Rev. Sci. Instrum. 77 (2006) 083106.
[16] S. Xu et al., Magnetic resonance imaging with an optical atomic magnetometer, Proc. Natl. Acad. Sci. USA 103 (2006) 12668–12671.
[17] I.M. Savukov, S.J. Seltzer, M.V. Romalis, Detection of NMR signals with a radio-frequency atomic magnetometer, JMR 185 (2007) 214–220.
[18] W.A. Edelstein, G.H. Glover, C.J. Hardy, R.W. Redington, The intrinsic signal-to-noise ratio in NMR imaging, Magn. Res. Med. 3 (1986) 604–618.
[19] I.M. Savukov, S.J. Seltzer, M.V. Romalis, K.L. Sauer, Tunable atomic magnetometer for detection of radio-frequency magnetic fields, Phys. Rev. Lett. 95 (2005) 063004.
[20] T.W. Kornack, S.J. Smullin, S.-K. Lee, M.V. Romalis, A low-noise ferrite magnetic shield, Appl. Phys. Lett. 90 (2007) 223501.
[21] J.D. Jackson, Classical Electrodynamics, third ed., John Willey and Sons Inc., 1999.
[22] Available from: <http://www.dlinstruments.com/products/pdf/565.pdf>.